iScience

CellPress
OPEN ACCESS

Article

The importance of proinflammatory failed-repair tubular epithelia as a predictor of diabetic kidney disease progression

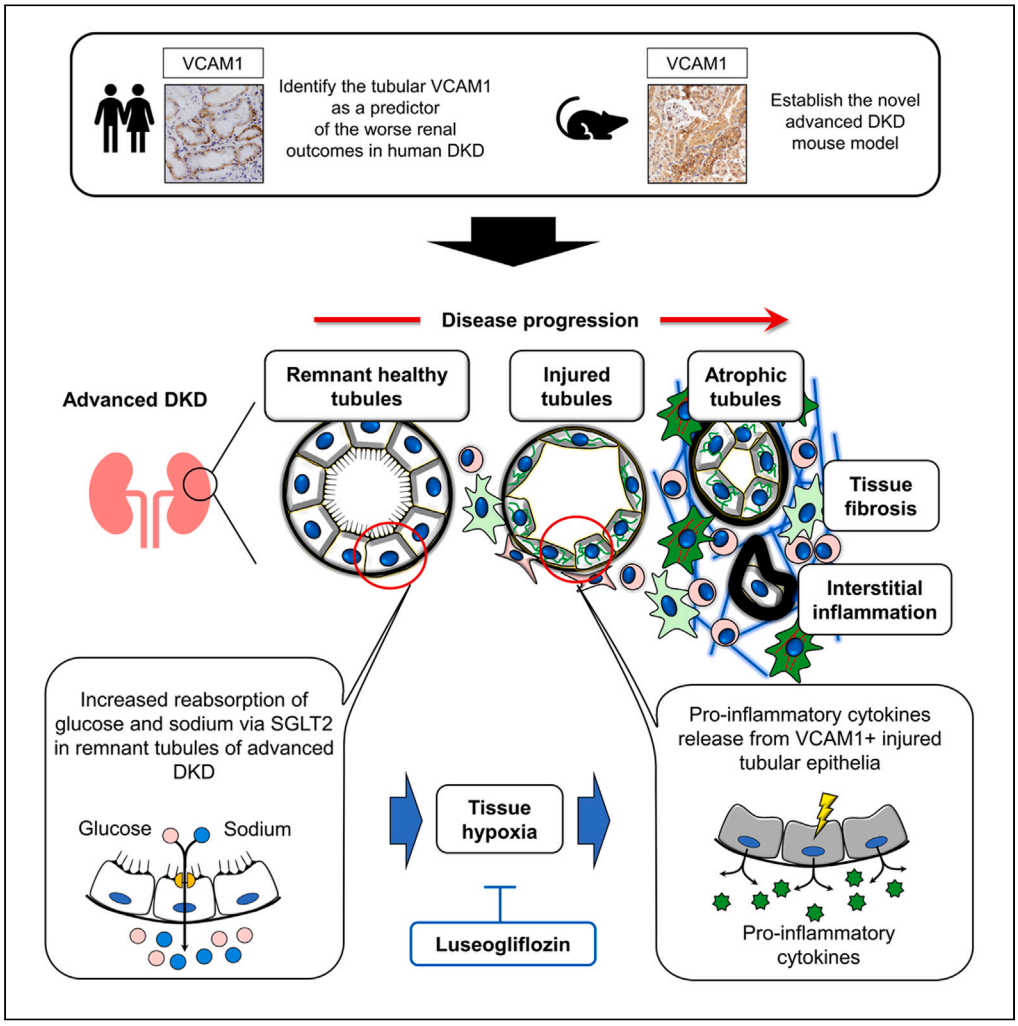

Aya Tomita-Yagi, Natsuko Ozeki-Okuno, Noriko Watanabe-Uehara, ..., Satoaki Matoba, Keiichi Tamagaki, Tetsuro Kusaba

kusaba@koto.kpu-m.ac.jp

Highlights

Tubular VCAM1 is potentially a useful histological marker for poor DKD outcomes

VCAM1+ tubules-mediated tissue injury may contribute to DKD progression

SGLT2 inhibitor improved renal histology in advanced DKD model

SGLT2 inhibitor reduced tubular VCAM1 expression by ameliorating tissue hypoxia

Tomita-Yagi et al., iScience 27, 109020
February 16, 2024
https://doi.org/10.1016/j.isci.2024.109020

iScience

CellPress
OPEN ACCESS

Article

The importance of proinflammatory failed-repair tubular epithelia as a predictor of diabetic kidney disease progression

Aya Tomita-Yagi,[1] Natsuko Ozeki-Okuno,[1] Noriko Watanabe-Uehara,[1] Kazumi Komaki,[1] Minato Umehara,[1] Hiroko Sawada-Yamauchi,[1] Atsushi Minamida,[1] Yasuto Sunahara,[1] Yayoi Matoba,[1] Itaru Nakamura,[1] Tomohiro Nakata,[1] Kunihiro Nakai,[1] Tomoharu Ida,[1] Noriyuki Yamashita,[1] Michitsugu Kamezaki,[1] Yuhei Kirita,[1] Takuya Taniguchi,[2] Eiichi Konishi,[3] Satoaki Matoba,[2] Keiichi Tamagaki,[1] and Tetsuro Kusaba[1,4,*]

SUMMARY

The immense public health burden of diabetic kidney disease (DKD) has led to an increase in research on the pathophysiology of advanced DKD. The present study focused on the significance of proinflammatory vascular cell adhesion molecule 1 (VCAM1)+ tubules in DKD progression. A retrospective cohort study of DKD patients showed that the percentage of VCAM1+ tubules in kidney samples was correlated with poor renal outcomes. We established an advanced DKD model by partial resection of the kidneys of *db/db* mice and demonstrated that it closely resembled the human advanced DKD phenotype, with tissue hypoxia, tubular DNA damage, tissue inflammation, and high tubular VCAM1 expression. Luseogliflozin ameliorated tissue hypoxia and proinflammatory responses, including VCAM1+ expression, in tubules. These findings suggest the potential of tubular VCAM1 as a histological marker for poor DKD outcomes. SGLT2 inhibitors may attenuate tissue hypoxia and subsequent tissue inflammation in advanced DKD, thereby ameliorating tubular injury.

INTRODUCTION

The recent development of sodium/glucose cotransporter 2 (SGLT2) inhibitors in clinical practice has resulted in better renal outcomes in patients with diabetic kidney disease (DKD) and non-diabetic chronic kidney disease (CKD). Large-scale clinical trials using various SGLT2 inhibitors and real-world evidence from the CKD registry revealed their renoprotective effects on early and advanced DKD.[1–7] Experimental investigations have offered various mechanistic insights into the renoprotective effects of SGLT2 inhibitors for early DKD through blood glucose lowering-dependent and -independent pathways,[8] such as reductions in oxidative stress,[9,10] improvements in glomerular hyperfiltration,[10,11] energy utilization by ketone body production,[12] and tissue hypoxia.[10,13] We and other researchers demonstrated that SGLT2 inhibitors attenuated decreases in tissue oxygen tension in the early diabetic kidney, which was attributed to the inhibition of sodium reabsorption reducing energy requirements through basolateral Na-K ATPase.[10,13–15]

In consideration of the complex etiology of advanced diabetic nephropathy, molecular phenotyping combined with detailed examinations of clinical phenotypes may provide insights into disease progression. Based on the significant improvements in renal outcomes by SGLT2 inhibitors reported in recent large-scale clinical trials and evidence that some patients with advanced DKD do not exhibit massive proteinuria or extensive diabetic glomerular lesions,[16] the major pathophysiology of DKD has shifted from a glomerulocentric to tubulocentric concept.[17–19] Due to the immense public health burden of diabetic nephropathy and subsequent end-stage renal disease, understanding the underlying molecular mechanisms has been at the forefront of diabetic renal disease research. However, since appropriate rodent models of advanced diabetic nephropathy manifesting as decreased kidney function, nodular glomerulosclerosis, and interstitial fibrosis have not yet been established,[20–23] the precise molecular mechanisms and preventative strategies for advanced DKD remain unclear.

Recent experimental findings, including single cell-based transcriptomics, revealed the expression of vascular cell adhesion molecule 1 (VCAM1) in the failed-repair tubular epithelia at the chronic phase after injury, which contributed to the transition from acute kidney injury (AKI) to CKD.[24,25] Proinflammatory cytokines, such as C-C motif chemokine ligand 2 (Ccl2), are released from VCAM1+ tubular epithelia, further exacerbating tissue injury. Therefore, we hypothesized that VCAM1+ tubular epithelia are also relevant for advanced DKD

[1]Department of Nephrology, Graduate School of Medical Science, Kyoto Prefectural University of Medicine, Kyoto, Japan
[2]Department of Cardiovascular Medicine, Graduate School of Medical Science, Kyoto Prefectural University of Medicine, Kyoto, Japan
[3]Department of Surgical Pathology, Graduate School of Medical Science, Kyoto Prefectural University of Medicine, Kyoto, Japan
[4]Lead contact
*Correspondence: kusaba@koto.kpu-m.ac.jp
https://doi.org/10.1016/j.isci.2024.109020

Table 1. Patient characteristics

	All DM patients (N = 24)	Low VCAM (N = 12)	High VCAM (N = 12)	p value
Age - yr	67.4 ± 8.1	67.8 ± 8.2	66.9 ± 8.2	0.787
Male sex - no. (%)	18 (75)	7 (58)	11 (91.7)	0.155
Body mass index - kg/m^2	25.1 ± 2.7	24.2 ± 2.7	26.0 ± 2.5	0.118
Diabetic retinopathy - no. (%)	10 (43.5)	4 (33.3)	6 (54.5)	0.414
Hypertesion - no. (%)	23 (95.8)	11 (91.7)	12 (100)	1
Smoking - no. (%)	18 (75)	6 (50)	12 (100)	0.014
HbA1c - % (interquartile range)	6.1 (5.8–6.9)	6.5 (5.9–6.9)	6.0 (5.7–6.8)	0.308
Cr - mg/dL (interquartile range)	1.33 (1.16–1.86)	1.32 (0.76–1.56)	1.69 (1.20–2.49)	0.139
eGFR - mL/min/1.73m^2 (interquartile range)	35.65 (28.93–46.08)	40.70 (32.05–63.68)	32.95 (22.98–43.80)	0.178
eGFR decline - ml/min/1.73m^2/year (interquartile range)	−7.55 (−10.9–−4.325)	−6.70 (−8.50–−3.90)	−8.34 (−14.48–−5.58)	0.075
U-Pro - g/gCr (interquartile range)	3.39 (1.77–11.03)	1.92 (0.74–8.46)	4.32 (2.50–12.75)	0.06
Hematuria - no. (%)	11 (45.8)	5 (41.7)	6 (50)	1
Insulin thrapy - no. (%)	3 (12.5)	0 (0)	3 (25)	0.217
Primary reason of renal biopsy				
Increased urinary protein - no. (%)	17 (70.8)	9 (75)	8 (66.7)	1
Positive urinary protein without diabetic retinopathy - no. (%)	4 (16.7)	1 (8.3)	3 (25)	0.59
Rapid decline in renal function - no. (%)	2 (8.3)	1 (8.3)	1 (8.3)	1
Kidney transplant donor - no. (%)	1 (4.2)	1 (8.3)	0 (0)	1

Plus-minus values are means ± SD. Data distribution was confirmed by the Shapiro-Wilk test. The unpaired *t*-test and Mann-Whitney test were performed for data analyses.

progression. We herein performed 5/6 nephrectomy on *db/db* mice, a type 2 diabetic mouse model, and established a novel advanced diabetic nephropathy model. Tissue hypoxia-DNA damage and proinflammatory responses through tubular VCAM1 expression were responsible for the development of severe histological lesions, which was confirmed in biopsy samples of human advanced diabetic nephropathy. Luseogloflozin, a SGLT2 inhibitor, mitigated renal histology in advanced diabetic nephropathy by attenuating tissue hypoxia and reducing tubular VCAM1 expression.

RESULTS

Tubular VCAM expression is a strong predictor of poor renal outcomes in DKD patients

In consideration of the emerging concept that VCAM1+ proinflammatory tubular epithelia contribute to CKD progression,[24,25] we investigated whether these cell populations are also present in human diabetic kidney tissues and associated with a poor renal prognosis. We performed immunostaining for VCAM1 in human biopsy samples obtained from 24 DKD patients and 4 thin basement membrane disease (TBMD) patients as a non-tubular injury control (Tables 1, S1, and S2). The results obtained showed that tubular VCAM1 expression was significantly higher in DKD patients than in TBMD patients, (Figures 1A and 1B). To analyze the impact of tubular VCAM1 expression on the renal outcomes of DKD patients, we divided DKD patients into the following groups: high (>42%, n = 12) and low (<42%, n = 12) VCAM1 expression. Regarding patient characteristics, the percentage of patients who were smokers and urinary protein levels were both higher in the high VCAM group (Tables 1 and S1). A renal histological analysis according to the American Society of Nephrology (ASN) criteria[26] showed that the glomerular score was higher in the high VCAM1 group (Figure 1C). We also examined glomerular lesions using another histology score (the NDT criteria)[27] and found that the scores for diffuse and nodular lesions were higher in the high VCAM1 group (Table S3). Regarding interstitial lesions, the score for interstitial fibrosis and tubular atrophy was higher in the high VCAM1 group (Figure 1D; Table S3). The score for interstitial inflammation in the ASN criteria was similar between the low and high VCAM1 groups, whereas the score in the NDT criteria was higher in the high VCAM group (Figure 1D; Table S3). Regarding vascular lesions, the scores for arteriolar hyalinosis and arteriosclerosis were similar between the high and low VCAM1 groups (Figure 1D; Table S3). We then investigated the impact of tubular VCAM1 positivity on renal outcomes (40% reduction in GFR, the induction of renal replacement therapy, and these combined outcomes). The cumulative renal composite outcomes free ratio was significantly lower in the high VCAM1 group (Figure 1E). The cumulative events-free ratio of each outcome was lower in the high VCAM1 group (Figures S1A and S1B). The cut-off point at 41.43% of VCAM1 positivity showed the highest likelihood values for sensitivity and specificity of the incidence of combined endpoints and a 40% reduction in eGFR (73.33 and 90% for combined endpoints, and 66.67 and 88.89% for a 40% reduction in eGFR, respectively. Figures 1F and S1C; Table S4). The cut-off point at 44.92% of VCAM1

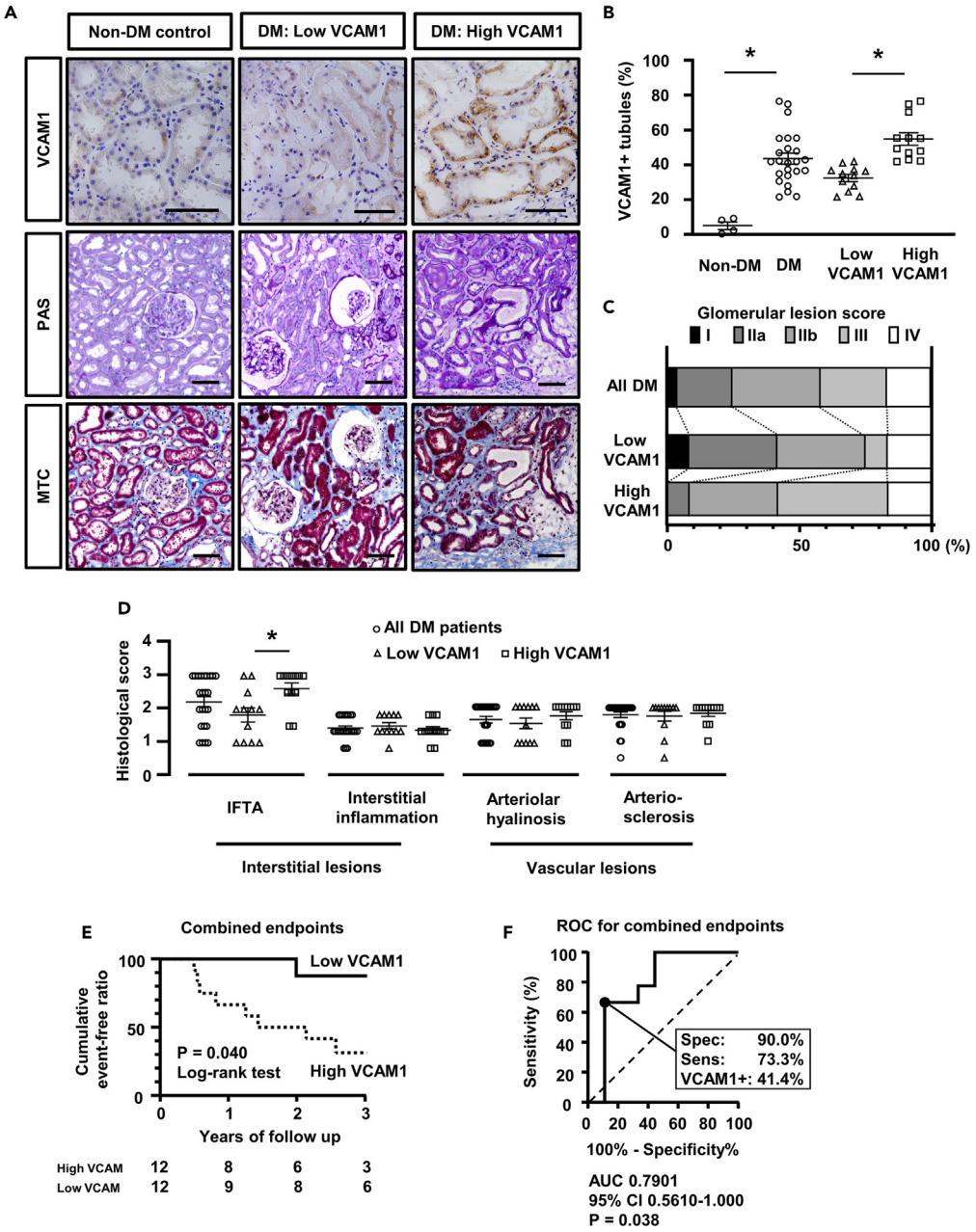

Figure 1. Tubular VCAM1 expression in human biopsy samples predicts the progression of DKD

(A) Representative images of immunostaining for VCAM1, PAS, and MTC. Bar, 50 μm.

(B) Comparative analysis of VCAM1+ tubules between non-DM and DM patients.

(C) Distribution of glomerular lesions in DKD patients.

(D) Quantification of the histological scores of interstitial and vascular lesions in DKD patients.

(E) Kaplan-Meier curve of the event-free ratio of composite renal outcomes in DKD patients.

(F) ROC curves of the percentage of VCAM1+ tubules for combined renal endpoints. In all groups, data are means ± SEM, Differences were calculated using unpaired t test in (B) and (D), and Log rank test in (E). *p < 0.05. See also Figure S1, Tables S1–S4.

positivity showed the highest likelihood values for sensitivity and specificity of the incidence of the induction of RRT (82.35 and 85.71%, respectively. Figure S1D; Table S4). Overall, an increase in tubular VCAM1 expression was a strong predictor of worse renal outcomes in DKD patients.

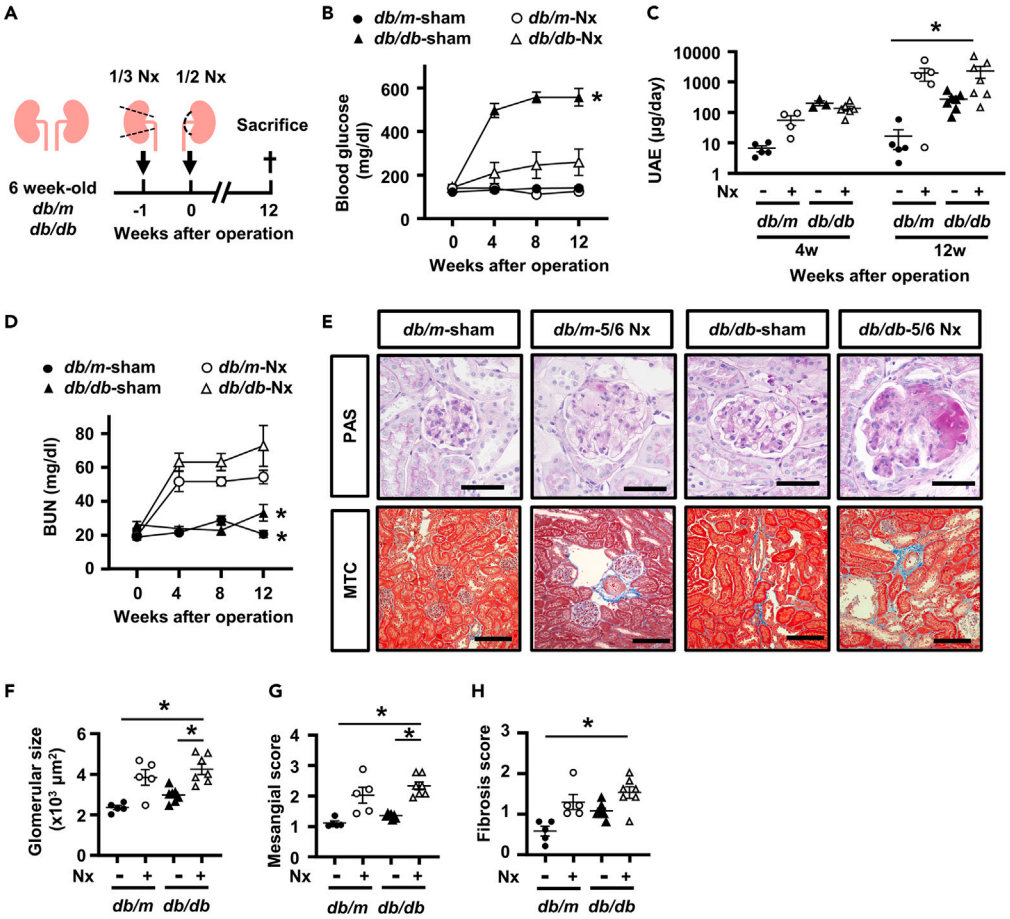

Figure 2. Generation of the novel DKD mouse model with reduced kidney function

(A) Scheme to generate the DKD model with reduced kidney function.

(B) Blood glucose levels over time after surgical procedures. (n = 5 to 7 each).

(C) Urinary albumin excretion (UAE) of experimental groups.

(D) BUN levels over time after surgical procedures. (n = 5 to 7 each).

(E) Representative pictures of PAS and MTC staining. Bar, 50 μm in PAS staining and 100 μm in MTC staining.

(F–H) Quantification of glomerular sizes, mesangial scores, and interstitial fibrosis in the experimental groups. In all groups, data are means ± SEM. Differences were calculated using the Kruskal-Wallis test in (B), (C), (D), (F), (G), and (H). *p < 0.05 vs. *db/db*-Nx mice. See also Figure S2A.

Generation of a novel diabetic mouse model with reduced renal function

To elucidate the underlying pathophysiology, we attempted to generate a rodent model of advanced DKD that accurately recapitulates the histology of human advanced DKD. Uninephrectomized diabetic mice were previously shown to develop diabetic glomerular lesions but not renal dysfunction.[28,29] Therefore, we resected the kidney and established a 5/6 nephrectomy model in *db/db* mice with renal dysfunction. To avoid operation-mediated lethality mainly caused by obesity and hyperglycemia, mouse kidneys were resected at 1-week intervals at the younger age of 6 weeks old (Figure 2A).[29,30] Hyperglycemia was noted in 5/6 nephrectomized *db/db* mice (*db/db*-Nx) but was less severe than in sham-operated *db/db* mice (*db/db*-sham) (Figure 2B), which is similar to DKD patients showing a spontaneous improvement in glycemic control according to the loss of renal function.[31] Body weight increased in *db/db*-sham and *db/db*-Nx mice (Figure S2A). Albuminuria significantly increased in *db/db*-Nx mice (Figure 2C). Regarding renal function, Nx-*db/db* mice and Nx-*db/m* mice showed a significant elevation in blood urea nitrogen (BUN) levels 1-week after 5/6 nephrectomy that remained at higher levels than those in sham-operated mice (Figure 2D).

Regarding renal histology after an observation period of 12 weeks, we found that glomerular sizes and mesangial matrix expansion were both significantly higher in *db/db*-Nx mice than in *db/db*-sham mice (Figures 2E–2G). MTC staining and a semiquantitative analysis showed interstitial fibrosis in *db/db*-Nx mice (Figures 2E and 2H). Given the strong phenotypes in *db/db*-Nx mice, including renal dysfunction, mesangial matrix expansion, and interstitial fibrosis, we considered this mouse model to successfully and accurately recapitulate advanced DKD in humans.[21]

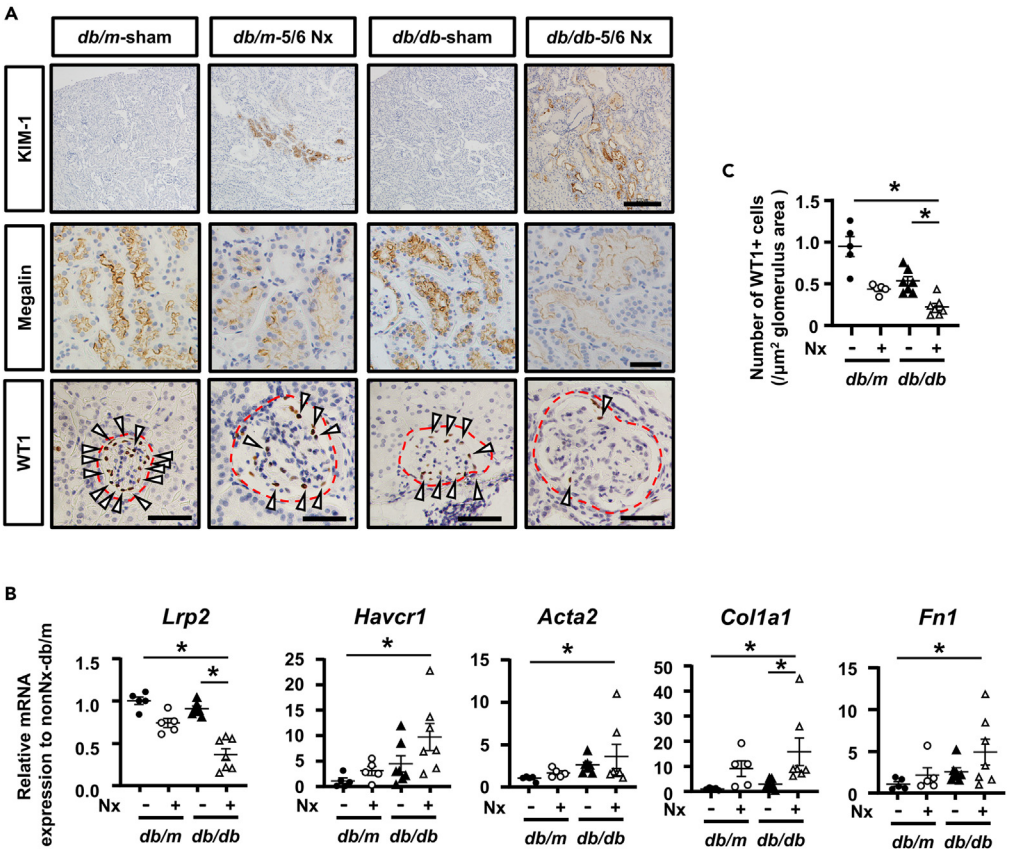

Figure 3. Detailed kidney tubular and podocyte injury in advanced DKD mice

(A) Immunostaining images for KIM-1, megalin, and WT1. Bar, 200 μm in KIM1 staining, 50 μm in megalin staining, and 20 μm in WT1 staining.

(B) qPCR of RNA from whole kidneys for the representative markers of mature tubules (*Lrp2*), of tubular injury (*Havcr1*), and profibrotic markers (*Col1a1*, *Acta2*, and *Fn1*).

(C) The density of WT1+ cells within the glomerulus. In all groups, data are means ± SEM, Differences were calculated using the Kruskal-Wallis test in (B) and (C). *p < 0.05 vs. *db/db*-Nx mice.

We then examined tubular and glomerular phenotypes in *db/db*-Nx mice. Immunostaining showed a significant increase in kidney injury marker-1 (KIM1), a tubular injury marker, and a significant reduction in megalin, a tubular integrity marker, in *db/db*-Nx mice (Figure 3A). We confirmed these phenotypes by qPCR, which also revealed a decrease in a healthy tubule marker (*Lrp2*, encoding megalin) and an increase in a tubular injury marker (*Havcr1*, encoding KIM1). qPCR also demonstrated an increase in tissue fibrosis markers (*Acta2*, *Col1a1*, and *Fn1*) in *db/db*-Nx mice (Figure 3B). Since the loss of podocytes is an important element of glomerulosclerosis and glomerular function in human DKD,[32,33] we examined the density of WT1-positive cells within the glomerulus, indicating healthy podocytes, and found that it was significantly reduced in *db/db*-Nx mice, suggesting the prominent loss of podocytes (Figures 3A and 3C). Regarding mesangial expansion, immunostaining for type 4 collagen showed the expansion of its positive area within glomeruli in *db/db*-Nx mice (Figure S3).

Tissue hypoxia and tubular proinflammatory responses in our advanced diabetic rodent model

Based on the significant relationship between tubular VCAM1 expression and poor renal outcomes in our analysis of human DKD, we performed immunostaining and qPCR for VCAM1 and found a marked increase in VCAM1+ tubules in *db/db*-Nx mice (Figures 4A and 4B). We also conducted immunostaining and qPCR for macrophage markers and found increases in F4/80 in immunostaining, and in RNA expressions of *Cd68* and *Ccl2* in *db/db*-Nx mice (Figures 4A and 4B). Co-staining for F4/80 and VCAM1 revealed marked increases in VCAM1+ tubules, which were surrounded by F4/80+ macrophages in *db/db*-Nx mice (Figure 4C). To elucidate the molecular mechanisms responsible for the development of advanced DKD in our model, we visualized tissue hypoxia by pimonidazole immunostaining because chronic hypoxia and oxidative stress are major contributors to disease progression in human CKD and DKD. The marked expansion of a pimonidazole-positive area was observed in *db/db*-Nx mice (Figures 4A and 4D). Concerning oxidative stress, another mechanism for the progression of DKD, immunostaining for 3-nitrotyrosine and Nox4 gene expression revealed no significant differences between experimental groups (Figure S4). We then assessed DNA damage using γH2AX immunostaining and found prominent DNA damage in the tubules, but not glomeruli, of *db/db*-Nx mice (Figures 4A, 4E, and S3). To examine the causal effects of hypoxia on VCAM expression in tubular epithelia, we performed an *in vitro*

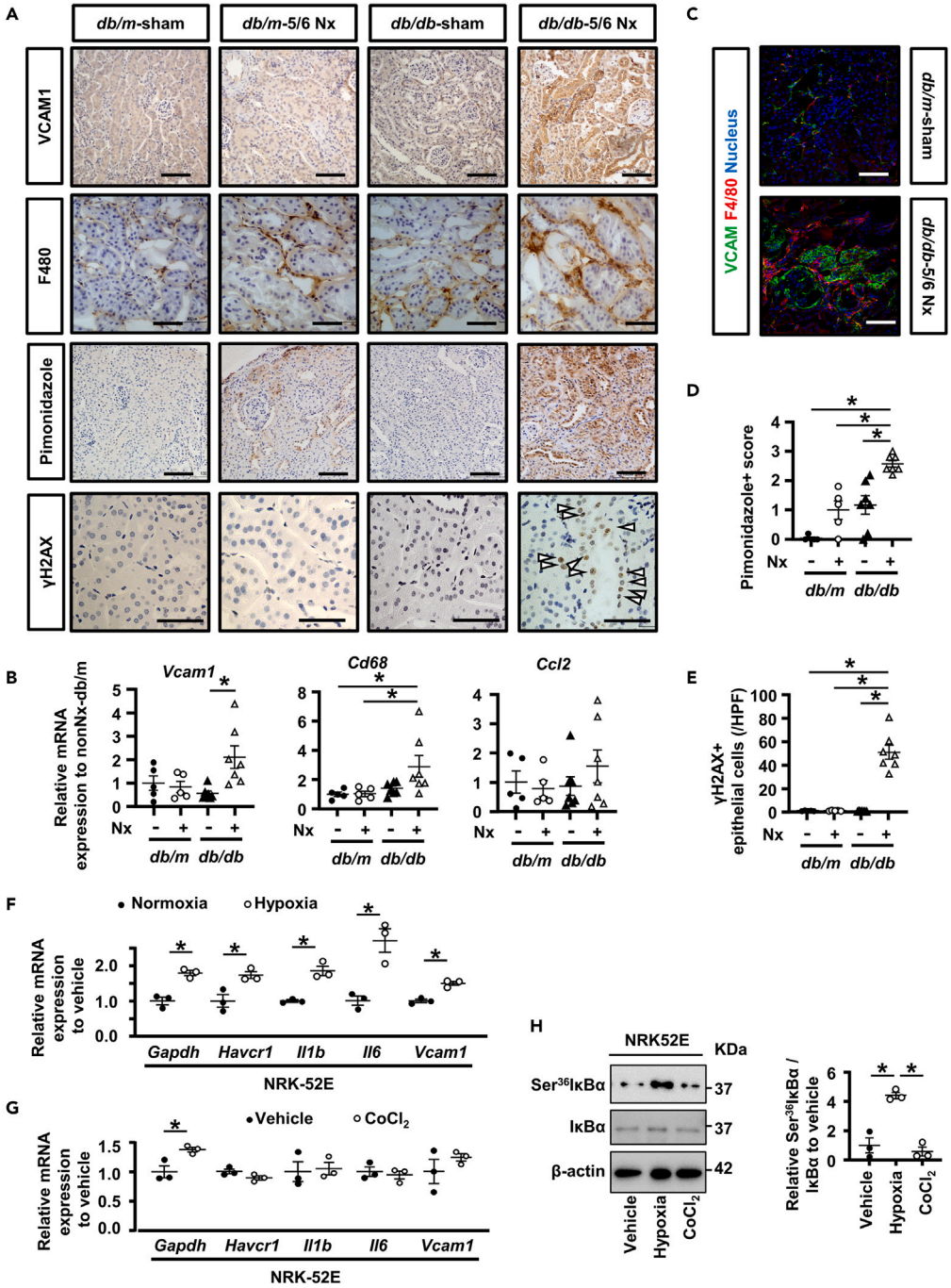

Figure 4. Tubular hypoxia, DNA damage, and VCAM1 expression in advanced DKD mice

(A) Representative immunostaining images for VCAM1, F4/80, pimonidazole, and γH2AX. Bar, 100 μm in pimonidazole and VCAM1 staining, and 50 μm in γH2AX and F4/80 staining.

(B) qPCR of RNA from whole kidneys for *Vcam1*, *Cd68*, and *Ccl2*.

(C) Immunofluorescence images of co-staining for VCAM1 and F4/80. Bar, 50 μm.

(D) Quantification of pimonidazole+ scores.

(E) Quantification of the number of gH2AX + tubular epithelial cells.

(F and G) qPCR of RNA from NRK-52E with exposure to hypoxia (F) and with the $CoCl_2$ treatment (G) for *Gapdh*, *Havcr1*, *Il1b*, *Il6*, *and Vcam1*.

(H) Western blot of protein lysates from NRK-52E for Ser^{34} IkBα, IkBα, and β-actin. A representative image of n = 1 for western blotting with n = 3 in each group is shown. The optical density of Ser^{34} IkBα bands was normalized against IkBα. The normalized density of samples from the vehicle treatment was arbitrarily set to 1. In all groups, data are means ± SEM. Differences were calculated using the Kruskal-Wallis test in (B), (D), (E), and (H), and using unpaired t test in (F) and (G). *$p < 0.05$ in (B), (D), (E), (F), (G), and (H). See also Figures S3, S4, and S6.

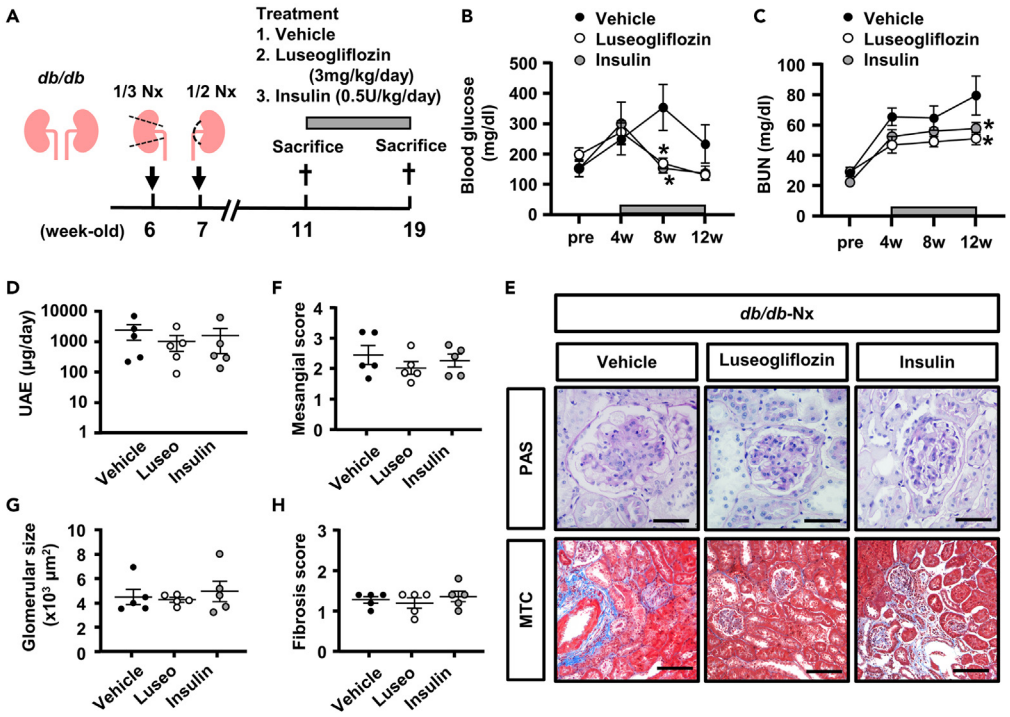

Figure 5. Luseogliflozin ameliorates tubular and glomerular injury in the advanced DKD model

(A) Scheme of the experimental schedule. During the treatment period, luseogliflozin (3 mg/kg/day) or insulin glargine (0.5 U/kg/day) was administered for 8 weeks.

(B and C) Blood glucose levels (B) and BUN levels (C) over time after surgical procedures and subsequent drug administration. (n = 5 to 7 each).

(D) Urinary albumin excretion (UAE) in experimental groups.

(E) Representative images of PAS and MTC staining. Bar, 50 μm in PAS staining and 100 μm in MTC staining.

(F–H) Quantification of mesangial scores (F), glomerular sizes (G), and fibrosis scores (H). In all groups, data are means ± SEM. Differences were calculated using the Kruskal-Wallis test in (B), (C), (D), (F), (G), and (H). *p < 0.05 vs. *db/db*-Nx mice with the vehicle treatment. See also Figure S2B.

analysis using NRK52E, a rat tubular epithelial cell line. After a 6-h exposure to hypoxia, *Gapdh*, one of the hypoxia-inducible factor (HIF) target genes, *Havcr1* (a tubular injury marker), *Il1b* and *Il6* (proinflammatory cytokines), and *Vcam1* were up-regulated in NRK52E (Figure 4F). To clarify whether the up-regulation of these genes was mediated by the activation of hypoxia-inducible factor (HIF), we performed qPCR after treatment with $CoCl_2$, a potent activator of HIF through inhibition of its degradation at cytoplasm. The expression of *Gapdh* was up-regulated by the $CoCl_2$ treatment, whereas that of *Havcr1*, *Il1b Il6*, and *Vcam1* was not (Figure 4G), indicating that the expression of *Vcam1* was not regulated by HIF. This result was supported by western blotting showing that NFkB was activated by exposure to hypoxia; however, this was not observed in $CoCl_2$-treated cells (Figures 4H and S6). We further analyzed the expressions of NFkB target genes *in vivo* and found that *Il1b* and *Il6* genes expression tended to increase in *db/db*-Nx mice (Figure S4B). Collectively, these results suggest that tubular hypoxia, active tubular injury, and subsequent VCAM1-mediated inflammatory responses were responsible for the development of strong phenotypes in our DKD model with reduced kidney function.

Effects of the luseogliflozin treatment on renal histology in the novel diabetic mouse model with reduced renal function

In consideration of the emerging positive impact of SGLT2 inhibitors on clinical outcomes in advanced DKD patients, we investigated whether luseogliflozin, an SGLT2 inhibitor, ameliorated the renal phenotypes in our DKD model with reduced kidney function. After an observation period of 4 weeks, luseogliflozin (3 mg/kg/day) was administered to *db/db*-Nx mice for 8 weeks (Figure 5A). To exclude a blood glucose-lowering effect, insulin glargine (0.5 U/kg/day) was administered to *db/db*-Nx mice for 8 weeks (Figure 5A). Blood glucose levels decreased to similar levels in luseogliflozin- and insulin-treated mice (Figure 5B). BUN gradually increased in vehicle-treated mice, whereas it remained at the same level in luseogliflzon- and insulin-treated mice (Figure 5C). Proteinuria was slightly less severe in luseogliflozin-treated mice (Figure 5D). Body weight did not gradually increase in any experimental group and did not significantly differ among the groups (Figure S2B). Regarding renal histology, mesangial matrix expansion was slightly ameliorated by the luseogliflozin treatment; however, there were no significant changes in glomerular hypertrophy or fibrosis (Figures 5E–5G).

Immunostaining showed that the expression of KIM1 decreased in luseogliflozin- and insulin-treated mice (Figure 6A). The expression of megalin markedly decreased in vehicle-treated mice but was preserved in luseogliflozin-treated mice (Figure 6A). Interstitial type 4 collagen expression was ameliorated in luseogliflozin-treated mice (Figure 6A). The qPCR analysis demonstrated that the mRNA expression of *Havcr1*,

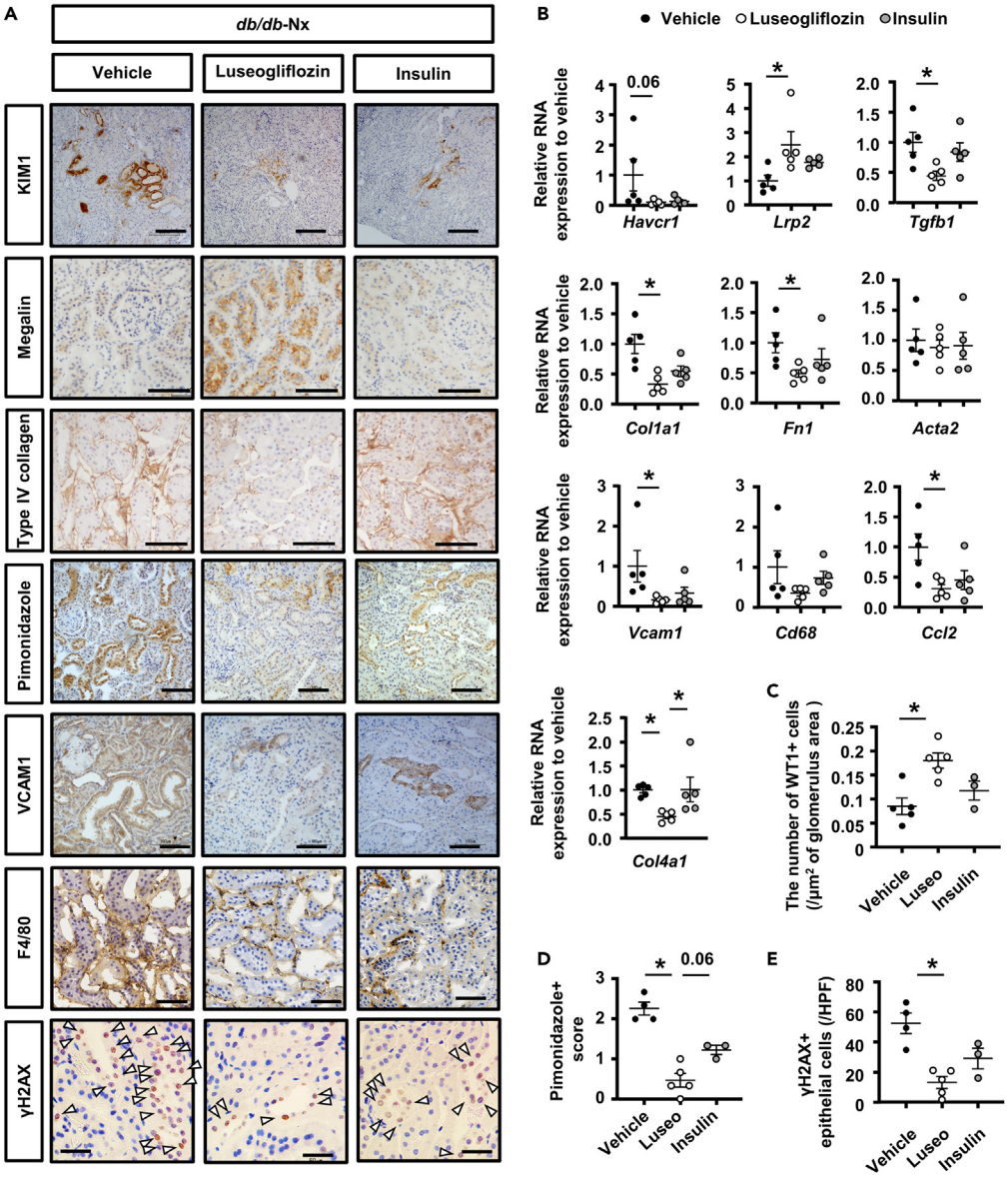

Figure 6. Luseogliflozin ameliorates tissue hypoxia, tubular DNA damage, and tubular VCAM1 expression

(A) Representative immunostaining images of KIM1, megalin, type IV collagen, pimonidazole, VCAM1, F4/80, and γH2AX. Arrowheads in γH2AX staining indicate the γH2AX-positive tubular epithelial cells, Bar, 200 μm in KIM1 staining, 100 μm in type IV collagen, pimonidazole and VCAM1 staining, 50 μm in megalin and F4/80 staining, and 20 μm in γH2AX staining.

(B) qPCR of RNA from whole kidneys for tubular injury, fibrosis, and inflammation markers.

(C) The density of WT1+ cells within the glomerulus.

(D) Quantification of pimonidazole+ scores.

(E) Quantification of the number of gH2AX + tubular epithelial cells. In all groups, data are means ± SEM. Differences were calculated using the Kruskal-Wallis test in (B), (C), (D), and (E). *p < 0.05 vs. *db/db*-Nx mice with the vehicle treatment. See also Figure S5.

Col1a1, *Fn1*, *Tgfb1*, and *Col4a1* was lower in luseogliflozin- and insulin-treated mice (Figure 6B), whereas that of *Lrp2* mRNA was higher in luseogliflozin-treated mice (Figure 6B). Regarding the effects of luseogliflozin on glomerular phenotypes, the number of WT1+ cells was higher and the glomerular expression of type 4 collagen was lower in luseogliflozin-treated mice (Figures 6C and S5).

Regarding the effects of luseogliflozin on tubular VCAM1 expression, immunostaining and qPCR revealed a decrease in VCAM1 expression in luseogliflozin-treated mice (Figures 6A and 6B). Immunostaining and qPCR for macrophage markers revealed slight reductions in luseogliflozin-treated mice (Figures 6A and 6B). Immunostaining to assess tissue hypoxia and DNA damage demonstrated that the pimonidazole-positive area and γH2AX + tubular epithelia were reduced by the luseogliflozin treatment (Figures 6A, 6C, and 6D). Concerning

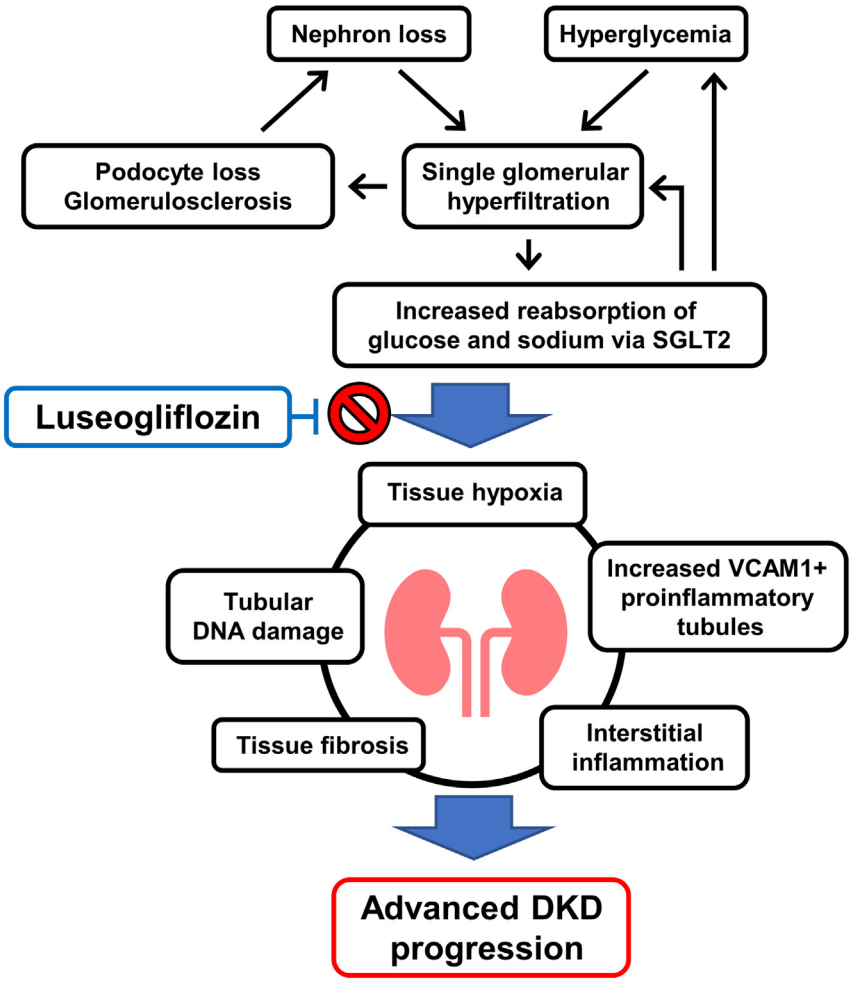

Figure 7. Proposed tubulocentric mechanism of advanced DKD progression and preventative effects by luseogliflozin.

glomerular phenotypes, positive F4/80 staining within glomeruli was ameliorated in luseogliflozin- and insulin-treated mice, whereas glomerular γH2AX + cells were not found in any experimental group (Figure S5).

DISCUSSION

In the present study, we generated a novel DKD mouse model with reduced kidney function by a simple surgical kidney mass reduction in *db/db* mice. This novel mouse model exhibited progressive renal insufficiency with DKD-specific histological characteristics, including extensive glomerular lesions and interstitial fibrosis. Regarding mechanistic histological phenotypes, tissue hypoxia, tubular DNA damage, and the development of proinflammatory VCAM1+ tubules were observed. VCAM1+ tubules were also detected in human DKD kidney samples, and tubular VCAM1 positivity was closely associated with worse renal outcomes. An SGLT2 inhibitor markedly attenuated tissue hypoxia and tubular DNA damage and reduced VCAM1 expression in our advanced DKD model, and these comprehensive and preventative mechanisms may explain the better renal outcomes achieved by SGLT2 inhibitors in advanced DKD (Figure 7).

In terms of the establishment of a novel mouse DKD model, the Animal Models of Diabetic Complications Consortium defined key criteria for ideal rodent models of advanced DKD, including overt albuminuria, the histopathological changes of glomerulosclerosis, and progressive renal insufficiency.[20,21] However, conventional diabetic mouse models only manifest moderate albuminuria and minimal histopathological changes, such as mild mesangial expansion and glomerular hypertrophy.[20–23] Although mouse lines incorporated with additional genetic stressors, including an endothelial nitric oxide synthase deficiency or chronic renin-angiotensin system activation, have been developed,[34–36] due to gene modifications and subsequent high blood pressure, these models do not accurately replicate the clinical manifestations of advanced DKD in humans.[20] To overcome these limitations, we developed a novel mouse DKD model with reduced kidney function by the simple surgical intervention of subtotal nephrectomy in *db/db* mice. Considering the balance between the maturation of kidney structures and avoidance of hyperglycemia or obesity-related high mortality during surgical procedures, previous studies performed uninephrectomy on *db/db* mice at 6 weeks old. Although the risk of hemorrhage in our model was considered to be higher than that of normal unilateral

nephrectomy because it involves the removal of renal tissue, we were able to perform surgery on mice with minimal mortality using 6-week-old mice.

A group of DKD patients with a rapid rate of renal function decline, called rapid decliners, have recently been identified, and their identification and countermeasures may be important for reducing the number of future dialysis patients. In the present study, we focused on VCAM1-positive failed-repair proximal tubule cells, which are inflammatory proximal tubules that fail to regenerate after injury, as identified by recent single-cell-based transcriptomics.[24] VCAM1-positive tubules secrete proinflammatory cytokines, such as CCl2, which induce the accumulation of macrophages after acute kidney injury caused by ischemia-reperfusion injury or repeated cisplatin injections, induce persistent tissue inflammation, and ultimately contribute to tissue injury.[24,25] In the present study, immunostaining on human DKD showed VCAM1-positive tubules, and their positivity was closely associated with a poor renal prognosis. The clinical findings of subjects revealed a difference in the reduction in eGFR between those with high VCAM1 and those with low VCAM1. The high percentage of VCAM1-positive tubules observed in the present study may be an important histological marker to stratify the risk of future DKD progression.

As observed in human DKD, VCAM1-positive tubules surrounded by infiltrated macrophages were also detected in our advanced DKD model. Luseogliflozin reduced the number of VCAM1+ tubules, and one possible molecular mechanism for this is the amelioration of tissue hypoxia. Due to high oxygen consumption and the specific structure of its microcirculation, the kidney is physiologically exposed to hypoxia, particularly at the cortico-medullary junction.[37,38] Regardless of primary pathophysiologies, this tissue hypoxic condition is accelerated under CKD, resulting in the further exacerbation of CKD.[37–39] Clinical evidence showing that SGLT2 inhibitors improve renal outcomes in non-DKD and DKD patients indicates a common SGLT2-mediated pathway for renal injury between these different disease entities and the drugs that act on it. In the early diabetic kidney, because of an increase in sodium reabsorption through SGLT2, the tissue hypoxic region expands toward the kidney cortex.[10,13,40–42] Advanced DKD contains the combined pathophysiologies of CKD and DKD; therefore, renal cortical tissue hypoxia was more evident in our novel advanced DKD mouse model than in Nx-*db/m* mice and non-Nx *db/db* mice. A recent study on the single cell-based transcriptomics of diabetic kidneys demonstrated that a hypoxic response was enhanced in the proximal tubules of the diabetic kidney, and an SGLT2 inhibitor reduced this signaling response.[36] Consistent with these findings, the present results demonstrated that luseogliflozin markedly reduced the hypoxic region in the kidney of our advanced DKD model. The results of *in vitro* experiments showing that hypoxia triggered the activation of NFkB signaling, including VCAM1 expression, in tubular epithelial cell lines indicate that the renoprotective effects of luseogliflozin are attributed to the amelioration of tissue hypoxia and a subsequent reduction in VCAM1.

In conclusion, we integrated human and mouse analyses and demonstrated the importance of proinflammatory VCAM1-positive tubular epithelia in the pathogenesis of advanced DKD. The SGLT2 inhibitor exerted renoprotective effects through the combined effects of ameliorating tissue hypoxia, reducing tubular DNA damage, and decreasing the number of VCAM1-expressing tubules, thereby attenuating subsequent tissue inflammation. These results may explain the significant reduction reported in the incidence of renal events in early and advanced DKD by SGLT2 inhibitors in recent large-scale clinical trials. Further investigations for gender differences and longer treatment duration on our established mouse model of advanced DKD will provide detailed insights into the pathophysiology of DKD progression and contribute to the development of preventative strategies.

Limitations of the study

One limitation of the present study is that hyperglycemia in our advanced DKD model was similar to that in *db/db* mice due to the suppression of increases in blood glucose levels caused by renal dysfunction. In diabetic patients with renal dysfunction, blood glucose levels are suppressed due to decreased gluconeogenesis in tubular epithelia and urinary insulin clearance,[43,44] and this may be the same phenomenon in our mouse model. Since advanced DKD develops in humans due to a long-term exposure to hyperglycemia, it was difficult to reproduce these effects on the histological changes in our mouse model. For example, previous studies reported that increased oxidative stress associated with hyperglycemia was important in the pathogenesis of diabetic nephropathy,[10,45] whereas in our model, the up-regulated expression of the *Nox4* gene and increased immunostaining for nitrotyrosine were lower than those in *db/db* mice, which may be attributed to lower blood glucose levels.

Another limitation is the precise intracellular molecular mechanisms by which the SGLT2 inhibitor exerted renoprotective effects remain unclear, and they ideally need to be investigated *in vitro*. Maintaining the cellular polarity of apical and basolateral sides is essential for SGLT2 expression on the cell surface of tubular epithelia.[46,47] However, cellular polarity is lost under culture conditions on a plastic dish, making it difficult to examine the detailed effects of SGLT2 inhibitors *in vitro*. In addition, one technical weakness of this study is that we did not include female mice in all experimental groups, thus, whether our conclusion can be generalized to the female mice is unclear.

STAR★METHODS

Detailed methods are provided in the online version of this paper and include the following:

- KEY RESOURCES TABLE
- RESOURCE AVAILABILITY
  - Lead contact
  - Materials availability

SUPPLEMENTAL INFORMATION

Supplemental information can be found online at https://doi.org/10.1016/j.isci.2024.109020.

ACKNOWLEDGMENTS

The present study, except for clinical investigations, was funded by an investigator-initiated grant from Taisho Pharmaceutical.

AUTHOR CONTRIBUTIONS

A.Y.-T. and T. K. designed the study, performed the experiments, analyzed the data, and wrote the manuscript. K.K. and T.T. analyzed the data. N.O.-O, N.U.-W., M.U., H.Y.-S, A.M., Y.S., Y.M., I.N., T.N., K.N., T.I., N.Y., M.K., Y.K., E.K., S.M., and K.T. analyzed the data and contributed to the discussion. K.T. and S.M. reviewed/edited the manuscript. T. K. has directly accessed and verified the underlying data reported in the manuscript.

DECLARATION OF INTERESTS

T. Kusaba reports receiving commercial research support from Taisho Pharmaceutical and speaker's bureau honoraria from AstraZeneca.

Received: July 27, 2023
Revised: November 17, 2023
Accepted: January 22, 2024
Published: January 26, 2024

REFERENCES

1. Heerspink, H.J.L., Stefánsson, B.V., Correa-Rotter, R., Chertow, G.M., Greene, T., Hou, F.F., Mann, J.F.E., McMurray, J.J.V., Lindberg, M., Rossing, P., et al. (2020). Dapagliflozin in Patients with Chronic Kidney Disease. N. Engl. J. Med. *383*, 1436–1446. https://doi.org/10.1056/NEJMoa2024816.
2. Perkovic, V., Jardine, M.J., Neal, B., Bompoint, S., Heerspink, H.J.L., Charytan, D.M., Edwards, R., Agarwal, R., Bakris, G., Bull, S., et al. (2019). Canagliflozin and Renal Outcomes in Type 2 Diabetes and Nephropathy. N. Engl. J. Med. *380*, 2295–2306. https://doi.org/10.1056/NEJMoa1811744.
3. Neal, B., Perkovic, V., Mahaffey, K.W., de Zeeuw, D., Fulcher, G., Erondu, N., Shaw, W., Law, G., Desai, M., and Matthews, D.R.; CANVAS Program Collaborative Group (2017). Canagliflozin and Cardiovascular and Renal Events in Type 2 Diabetes. N. Engl. J. Med. *377*, 644–657. https://doi.org/10.1056/NEJMoa1611925.
4. Wanner, C., Inzucchi, S.E., Lachin, J.M., Fitchett, D., von Eynatten, M., Mattheus, M., Johansen, O.E., Woerle, H.J., Broedl, U.C., and Zinman, B.; EMPA-REG OUTCOME Investigators (2016). Empagliflozin and Progression of Kidney Disease in Type 2 Diabetes. N. Engl. J. Med. *375*, 323–334. https://doi.org/10.1056/NEJMoa1515920.
5. The EMPA-KIDNEY Collaborative Group, Herrington, W.G., Staplin, N., Wanner, C., Green, J.B., Hauske, S.J., Emberson, J.R., Preiss, D., Judge, P., Mayne, K.J., et al. (2023). Empagliflozin in Patients with Chronic Kidney Disease. N. Engl. J. Med. *388*, 117–127. https://doi.org/10.1056/NEJMoa2204233.
6. Heerspink, H.J.L., Karasik, A., Thuresson, M., Melzer-Cohen, C., Chodick, G., Khunti, K., Wilding, J.P.H., Garcia Rodriguez, L.A., Cea-Soriano, L., Kohsaka, S., et al. (2020). Kidney outcomes associated with use of SGLT2 inhibitors in real-world clinical practice (CVD-REAL 3): a multinational observational cohort study. Lancet Diabetes Endocrinol. *8*, 27–35. https://doi.org/10.1016/S2213-8587(19)30384-5.
7. Nagasu, H., Yano, Y., Kanegae, H., Heerspink, H.J.L., Nangaku, M., Hirakawa, Y., Sugawara, Y., Nakagawa, N., Tani, Y., Wada, J., et al. (2021). Kidney Outcomes Associated With SGLT2 Inhibitors Versus Other Glucose-Lowering Drugs in Real-world Clinical Practice: The Japan Chronic Kidney Disease Database. Diabetes Care *44*, 2542–2551. https://doi.org/10.2337/dc21-1081.
8. DeFronzo, R.A., Reeves, W.B., and Awad, A.S. (2021). Pathophysiology of diabetic kidney disease: impact of SGLT2 inhibitors. Nat. Rev. Nephrol. *17*, 319–334. https://doi.org/10.1038/s41581-021-00393-8.
9. Tanaka, S., Sugiura, Y., Saito, H., Sugahara, M., Higashijima, Y., Yamaguchi, J., Inagi, R., Suematsu, M., Nangaku, M., and Tanaka, T. (2018). Sodium-glucose cotransporter 2 inhibition normalizes glucose metabolism and suppresses oxidative stress in the kidneys of diabetic mice. Kidney Int. *94*, 912–925. https://doi.org/10.1016/j.kint.2018.04.025.
10. Kamezaki, M., Kusaba, T., Komaki, K., Fushimura, Y., Watanabe, N., Ikeda, K., Kitani, T., Yamashita, N., Uehara, M., Kirita, Y., et al. (2018). Comprehensive renoprotective effects of ipragliflozin on early diabetic nephropathy in mice. Sci. Rep. *8*, 4029. https://doi.org/10.1038/s41598-018-22229-5.

11. Kidokoro, K., Cherney, D.Z.I., Bozovic, A., Nagasu, H., Satoh, M., Kanda, E., Sasaki, T., and Kashihara, N. (2019). Evaluation of Glomerular Hemodynamic Function by Empagliflozin in Diabetic Mice Using In Vivo Imaging. Circulation *140*, 303–315. https://doi.org/10.1161/CIRCULATIONAHA.118.037418.
12. Tomita, I., Kume, S., Sugahara, S., Osawa, N., Yamahara, K., Yasuda-Yamahara, M., Takeda, N., Chin-Kanasaki, M., Kaneko, T., Mayoux, E., et al. (2020). SGLT2 Inhibition Mediates Protection from Diabetic Kidney Disease by Promoting Ketone Body-Induced mTORC1 Inhibition. Cell Metab. *32*, 404–419.e6. https://doi.org/10.1016/j.cmet.2020.06.020.
13. Uehara-Watanabe, N., Okuno-Ozeki, N., Nakamura, I., Nakata, T., Nakai, K., Yagi-Tomita, A., Ida, T., Yamashita, N., Kamezaki, M., Kirita, Y., et al. (2022). Proximal tubular epithelia-specific transcriptomics of diabetic mice treated with dapagliflozin. Heliyon *8*, e10615. https://doi.org/10.1016/j.heliyon.2022.e10615.
14. Körner, A., Eklöf, A.C., Celsi, G., and Aperia, A. (1994). Increased renal metabolism in diabetes. Mechanism and functional implications. Diabetes *43*, 629–633.
15. O'Neill, J., Fasching, A., Pihl, L., Patinha, D., Franzen, S., and Palm, F. (2015). Acute SGLT inhibition normalizes O2 tension in the renal cortex but causes hypoxia in the renal medulla in anaesthetized control and diabetic rats. Am. J. Physiol. Renal Physiol. *309*, F227–F234. https://doi.org/10.1152/ajprenal.00689.2014.
16. Krolewski, A.S. (2015). Progressive renal decline: the new paradigm of diabetic nephropathy in type 1 diabetes. Diabetes Care *38*, 954–962. https://doi.org/10.2337/dc15-0184.
17. Gilbert, R.E. (2017). Proximal Tubulopathy: Prime Mover and Key Therapeutic Target in Diabetic Kidney Disease. Diabetes *66*, 791–800. https://doi.org/10.2337/db16-0796.
18. Zeni, L., Norden, A.G.W., Cancarini, G., and Unwin, R.J. (2017). A more tubulocentric view of diabetic kidney disease. J. Nephrol. *30*, 701–717. https://doi.org/10.1007/s40620-017-0423-9.
19. Vallon, V., and Thomson, S.C. (2020). The tubular hypothesis of nephron filtration and diabetic kidney disease. Nat. Rev. Nephrol. *16*, 317–336. https://doi.org/10.1038/s41581-020-0256-y.
20. Azushima, K., Gurley, S.B., and Coffman, T.M. (2018). Modelling diabetic nephropathy in mice. Nat. Rev. Nephrol. *14*, 48–56. https://doi.org/10.1038/nrneph.2017.142.
21. Brosius, F.C., 3rd, Alpers, C.E., Bottinger, E.P., Breyer, M.D., Coffman, T.M., Gurley, S.B., Harris, R.C., Kakoki, M., Kretzler, M., Leiter, E.H., et al. (2009). Mouse models of diabetic nephropathy. J. Am. Soc. Nephrol. *20*, 2503–2512. https://doi.org/10.1681/ASN.2009070721.
22. Kitada, M., Ogura, Y., and Koya, D. (2016). Rodent models of diabetic nephropathy: their utility and limitations. Int. J. Nephrol. Renovasc. Dis. *9*, 279–290. https://doi.org/10.2147/IJNRD.S103784.
23. Giralt-López, A., Molina-Van den Bosch, M., Vergara, A., García-Carro, C., Seron, D., Jacobs-Cachá, C., and Soler, M.J. (2020). Revisiting Experimental Models of Diabetic Nephropathy. Int. J. Mol. Sci. *21*, 3587. https://doi.org/10.3390/ijms21103587.
24. Kirita, Y., Wu, H., Uchimura, K., Wilson, P.C., and Humphreys, B.D. (2020). Cell profiling of mouse acute kidney injury reveals conserved cellular responses to injury. Proc. Natl. Acad. Sci. USA *117*, 15874–15883. https://doi.org/10.1073/pnas.2005477117.
25. Yamashita, N., Nakai, K., Nakata, T., Nakamura, I., Kirita, Y., Matoba, S., Humphreys, B.D., Tamagaki, K., and Kusaba, T. (2021). Cumulative DNA damage by repeated low-dose cisplatin injection promotes the transition of acute to chronic kidney injury in mice. Sci. Rep. *11*, 20920. https://doi.org/10.1038/s41598-021-00392-6.
26. Tervaert, T.W.C., Mooyaart, A.L., Amann, K., Cohen, A.H., Cook, H.T., Drachenberg, C.B., Ferrario, F., Fogo, A.B., Haas, M., de Heer, E., et al. (2010). Pathologic classification of diabetic nephropathy. J. Am. Soc. Nephrol. *21*, 556–563. https://doi.org/10.1681/ASN.2010010010.
27. Furuichi, K., Yuzawa, Y., Shimizu, M., Hara, A., Toyama, T., Kitamura, H., Suzuki, Y., Sato, H., Uesugi, N., Ubara, Y., et al. (2018). Nationwide multicentre kidney biopsy study of Japanese patients with type 2 diabetes. Nephrol. Dial. Transplant. *33*, 138–148. https://doi.org/10.1093/ndt/gfw417.
28. Tahara, A., and Takasu, T. (2018). Prevention of progression of diabetic nephropathy by the SGLT2 inhibitor ipragliflozin in uninephrectomized type 2 diabetic mice. Eur. J. Pharmacol. *830*, 68–75. https://doi.org/10.1016/j.ejphar.2018.04.024.
29. Motrapu, M., Świderska, M.K., Mesas, I., Marschner, J.A., Lei, Y., Martinez Valenzuela, L., Fu, J., Lee, K., Angelotti, M.L., Antonelli, G., et al. (2020). Drug Testing for Residual Progression of Diabetic Kidney Disease in Mice Beyond Therapy with Metformin, Ramipril, and Empagliflozin. J. Am. Soc. Nephrol. *31*, 1729–1745. https://doi.org/10.1681/ASN.2019070703.
30. Sayyed, S.G., Ryu, M., Kulkarni, O.P., Schmid, H., Lichtnekert, J., Grüner, S., Green, L., Mattei, P., Hartmann, G., and Anders, H.J. (2011). An orally active chemokine receptor CCR2 antagonist prevents glomerulosclerosis and renal failure in type 2 diabetes. Kidney Int. *80*, 68–78. https://doi.org/10.1038/ki.2011.102.
31. Kalantar-Zadeh, K., Derose, S.F., Nicholas, S., Benner, D., Sharma, K., and Kovesdy, C.P. (2009). Burnt-out diabetes: impact of chronic kidney disease progression on the natural course of diabetes mellitus. J. Ren. Nutr. *19*, 33–37. https://doi.org/10.1053/j.jrn.2008.11.012.
32. Pagtalunan, M.E., Miller, P.L., Jumping-Eagle, S., Nelson, R.G., Myers, B.D., Rennke, H.G., Coplon, N.S., Sun, L., and Meyer, T.W. (1997). Podocyte loss and progressive glomerular injury in type II diabetes. J. Clin. Invest. *99*, 342–348. https://doi.org/10.1172/JCI119163.
33. White, K.E., Bilous, R.W., Marshall, S.M., El Nahas, M., Remuzzi, G., Piras, G., De Cosmo, S., and Viberti, G. (2002). Podocyte number in normotensive type 1 diabetic patients with albuminuria. Diabetes *51*, 3083–3089. https://doi.org/10.2337/diabetes.51.10.3083.
34. Zhao, H.J., Wang, S., Cheng, H., Zhang, M.Z., Takahashi, T., Fogo, A.B., Breyer, M.D., and Harris, R.C. (2006). Endothelial nitric oxide synthase deficiency produces accelerated nephropathy in diabetic mice. J. Am. Soc. Nephrol. *17*, 2664–2669. https://doi.org/10.1681/ASN.2006070798.
35. Thibodeau, J.F., Holterman, C.E., Burger, D., Read, N.C., Reudelhuber, T.L., and Kennedy, C.R.J. (2014). A novel mouse model of advanced diabetic kidney disease. PLoS One *9*, e113459. https://doi.org/10.1371/journal.pone.0113459.
36. Wu, H., Gonzalez Villalobos, R., Yao, X., Reilly, D., Chen, T., Rankin, M., Myshkin, E., Breyer, M.D., and Humphreys, B.D. (2022). Mapping the single-cell transcriptomic response of murine diabetic kidney disease to therapies. Cell Metab. *34*, 1064–1078.e6. https://doi.org/10.1016/j.cmet.2022.05.010.
37. Nangaku, M. (2006). Chronic hypoxia and tubulointerstitial injury: a final common pathway to end-stage renal failure. J. Am. Soc. Nephrol. *17*, 17–25. https://doi.org/10.1681/ASN.2005070757.
38. Heyman, S.N., Khamaisi, M., Rosen, S., and Rosenberger, C. (2008). Renal parenchymal hypoxia, hypoxia response and the progression of chronic kidney disease. Am. J. Nephrol. *28*, 998–1006. https://doi.org/10.1159/000146075.
39. Hirakawa, Y., Tanaka, T., and Nangaku, M. (2017). Renal Hypoxia in CKD; Pathophysiology and Detecting Methods. Front. Physiol. *8*, 99. https://doi.org/10.3389/fphys.2017.00099.
40. Shibata, R., Ueda, S., Yamagishi, S., Kaida, Y., Matsumoto, Y., Fukami, K., Hayashida, A., Matsuoka, H., Kato, S., Kimoto, M., and Okuda, S. (2009). Involvement of asymmetric dimethylarginine (ADMA) in tubulointerstitial ischaemia in the early phase of diabetic nephropathy. Nephrol. Dial. Transplant. *24*, 1162–1169. https://doi.org/10.1093/ndt/gfn630.
41. Takiyama, Y., Harumi, T., Watanabe, J., Fujita, Y., Honjo, J., Shimizu, N., Makino, Y., and Haneda, M. (2011). Tubular injury in a rat model of type 2 diabetes is prevented by metformin: a possible role of HIF-1alpha expression and oxygen metabolism. Diabetes *60*, 981–992. https://doi.org/10.2337/db10-0655.
42. Uehara-Watanabe, N., Okuno-Ozeki, N., Minamida, A., Nakamura, I., Nakata, T., Nakai, K., Yagi-Tomita, A., Ida, T., Ikeda, K., Kitani, T., et al. (2022). Direct evidence of proximal tubular proliferation in early diabetic nephropathy. Sci. Rep. *12*, 778. https://doi.org/10.1038/s41598-022-04880-1.
43. Garla, V., Yanes-Cardozo, L., and Lien, L.F. (2017). Current therapeutic approaches in the management of hyperglycemia in chronic renal disease. Rev. Endocr. Metab. Disord. *18*, 5–19. https://doi.org/10.1007/s11154-017-9416-1.
44. Alsahli, M., and Gerich, J.E. (2017). Renal glucose metabolism in normal physiological conditions and in diabetes. Diabetes Res. Clin. Pract. *133*, 1–9. https://doi.org/10.1016/j.diabres.2017.07.033.
45. Coughlan, M.T., and Sharma, K. (2016). Challenging the dogma of mitochondrial reactive oxygen species overproduction in diabetic kidney disease. Kidney Int. *90*, 272–279. https://doi.org/10.1016/j.kint.2016.02.043.
46. Takesue, H., Hirota, T., Tachimura, M., Tokashiki, A., and Ieiri, I. (2018). Nucleosome Positioning and Gene Regulation of the SGLT2 Gene in the Renal Proximal Tubular Epithelial Cells. Mol. Pharmacol. *94*,

953–962. https://doi.org/10.1124/mol.118.111807.

47. Umino, H., Hasegawa, K., Minakuchi, H., Muraoka, H., Kawaguchi, T., Kanda, T., Tokuyama, H., Wakino, S., and Itoh, H. (2018). High Basolateral Glucose Increases Sodium-Glucose Cotransporter 2 and Reduces Sirtuin-1 in Renal Tubules through Glucose Transporter-2 Detection. Sci. Rep. *8*, 6791. https://doi.org/10.1038/s41598-018-25054-y.

48. Matsuo, S., Imai, E., Horio, M., Yasuda, Y., Tomita, K., Nitta, K., Yamagata, K., Tomino, Y., Yokoyama, H., and Hishida, A.; Collaborators developing the Japanese equation for estimated GFR (2009). Revised equations for estimated GFR from serum creatinine in Japan. Am. J. Kidney Dis. *53*, 982–992. https://doi.org/10.1053/j.ajkd.2008.12.034.

49. Uzzo, M., Moroni, G., and Ponticelli, C. (2023). Thin Basement Membrane: An Underrated Cause of End-Stage Renal Disease. Nephron *147*, 383–391. https://doi.org/10.1159/000528243.

50. Ida, T., Kusaba, T., Kado, H., Taniguchi, T., Hatta, T., Matoba, S., and Tamagaki, K. (2019). Ambulatory blood pressure monitoring-based analysis of long-term outcomes for kidney disease progression. Sci. Rep. *9*, 19296. https://doi.org/10.1038/s41598-019-55732-4.

STAR★METHODS

KEY RESOURCES TABLE

REAGENT or RESOURCE	SOURCE	IDENTIFIER
Antibodies		
KIM-1	R&D	Cat# AF1817; RRID:AB_2116446
Megalin	abcam	Cat# ab76969; RRID:AB_10673466
Type 4 collagen	abcam	Cat# ab6586; RRID:AB_305584
F4/80	abcam	Cat# ab6640; RRID:AB_1140040
VCAM-1	abcam	Cat# ab13047
WT-1	abcam	Cat# ab89901; RRID:AB_2043201
pimonidazole	Natural Pharmacia International	Cat# PAb2627; RRID:AB_1576904
Phospho-Histone H2A.X	Cell Signaling Technology	Cat# 2577S; RRID:AB_2118010
Nitrotyrosine	Merck Millipore	Cat# 06–284; RRID:AB_310089
Goat anti-rabbit HRP Conjugate	abcam	Cat# ab236469; Lot:GR3388394-1
mouse anti-goat IgG-HRP	Santa Cruz Biotechnology	Cat# sc-2354; RRID:AB_628490
goat anti-rat IgG-HRP	Santa Cruz Biotechnology	Cat# sc-2006; L RRID: AB_1125219
Anti-mouse IgG, HRP-linked Antibody	Cell Signaling Technology	Cat# 7076S RRID:AB_330924
Anti-rabbit IgG, HRP-linked Antibody	Cell Signaling Technology	Cat# 7074S RRID:AB_2099233
Chemicals, peptides, and recombinant proteins		
4% Paraformaldehyde Phosphate Buffer Solution	FUJIFILM	Code# 163–20145; Lot: M3K6675
Phosphate Buffered Saline	Takara Bio	Cat# T9181; Lot:AM2P017
Sucrose	FUJIFILM	Code# 196-00015; Lot: WTG4583
Optimum cutting temperature compound	SAKURA	Code# 4583; Lot.3806-00
Albumin, Bovine Serum (BSA)	NACALAI TESQUE	Code# 01860-07; Lot: M3K6675
Gelatin from cold water fish skin	Sigma-Aldrich	Cat# G7765; Lot:SLBG3980V
Polyoxyethylene(10) Octylphenyl Ether	FUJIFILM	Code# 168–11805; Lot:KCP6306
DAPI Fluoromount-G	Southern Biotech	Cat# 0100-20; Lot:J1120-X680B
diaminobenzidine chromogenic substrate	Agilent Technologies, Inc.	Code# K3468; Lot:11354051
Dulbecco's Minimal Essential Medium	Wako	N/A
lysing Buffer 17	R&D Systems, Inc.	Cat# 895943
Immobilon-P	Millipore	Cat# IPVH00010
ECL select Western blot detection reagent	GE Healthcare UK Ltd.	Cat# RPN2235
Clarity Max Western ECL substrate	Bio-Rad Laboratories, Inc.	Cat# 1705062
TRIzol	Life Technologies, Inc.	N/A
Insulin Glargine	FUJIFILM	Code# 092–06181 Lot:SKP4648
Luseogliflozin	Taisho Pharmaceutical Holdings Co.	N/A
Critical commercial assays		
Hypoxyprobe™-1 Omni Kit	Natural Pharmacia International	Item# HP3-100Kit; Lot:102822
Direct-zol RNA Miniprep	Zymo Research Corporation.	Cat# R2051
PrimeScript RT reagent Kit	Takara Bio Inc.	N/A
KAPA SYBR FAST Universal qPCR Kit	Kapa Biosystems	Ref# KK4602 Lot:0000240086
Experimental models: Cell lines		
Rat kidney epithelial cells (NRK 52E cells)	the JCRB Cell Bank	N/A

(*Continued on next page*)

Continued

REAGENT or RESOURCE	SOURCE	IDENTIFIER
Experimental models: Organisms/strains		
Mouse: BKS.Cg-Dock7m+/+Leprdb/J (Homozygote:db/db, heterozygote:db/m)	Oriental Bio Service Inc.	N/A
Oligonucleotides		
Primers see Table S5	This paper	N/A
Software and algorithms		
ImageJ software	National Institutes of Health	java.version: 1.8.0_391
BZ-X800	Keyence	BZ Series Application 01.02.03.02
Thermal Cycler Dice Real Time System	Takara Bio Inc.	N/A
Bio-Rad CFX Maestro	Bio-Rad Laboratories, Inc.	Version: 4.1.2433.1219
PRISM	GraphPad Software	Version 8.4.3
Eclipse E600 microscope	Nikon Corporation	N/A

RESOURCE AVAILABILITY

Lead contact

Further information and requests for resources should be directed to the lead contact, Dr. Tetsuro Kusaba (kusaba@koto.kpu-m.ac.jp).

Materials availability

This study did not generate new unique reagents.

Data and code availability

- All data reported in this paper will be shared by the lead contact upon request.
- This paper does not report original code.
- Any additional information required to reanalyze the data reported in this paper is available from the lead contact upon request.

EXPERIMENTAL MODEL AND STUDY PARTICIPANT DETAILS

For animal study, we purchased male diabetic BKS.Cg-Dock7m+/+Leprdb/J (*db/db*) mice and non-diabetic heterozygote (*db/m*) mice aged 6 weeks from Oriental Bio Service Inc. (Kyoto, Japan). 5 mice were housed in one cage under a 12-h light/dark cycle with free access to tap water and standard chow (CE-2, CLEA Japan, Inc., Tokyo, Japan). At the age of 6 weeks, male *db/db* or *db/m* mice were anesthetized with pentobarbital and unilateral kidney removal was performed by the retroperitoneal approach. One week later, at the age of 7 weeks, mice were anesthetized and resection of upper and lower poles of the right kidney was conducted by the retroperitoneal approach. Each experimental group contained 5 mice. All experiments were approved by the Experimental Animals Committee, Kyoto Prefectural University of Medicine (Approval number: M2022-122), and were performed in accordance with the institutional guidelines and Guidelines for Proper Conduct of Animal Experiments by the Science Council of Japan.

For human retrospective cohort study, we conducted that at the University Hospital of the Kyoto Prefectural University of Medicine in Kyoto Prefecture, Japan. We retrospectively enrolled 24 diabetic patients and 4 non-diabetic patients who underwent renal biopsy at Kyoto Prefectural University of Medicine. Clinical characteristics were collected from medical records, including age, sex, complications, primary reason of renal biopsy, laboratory results, which were performed within 2 weeks of the renal biopsy, and are listed in Table S1. The body mass index was defined as [weight (kg)]/[height (meters)]2. eGFR was calculated according to the following formula[48]: "194 × [age (years)]−0.287 × [serum creatinine (mg/dL)]−1.094 × [0.739 if female]". eGFR decline was calculated as the difference from the eGFR one year before the renal biopsy. As a control, we analyzed non-diabetic patients with thin basement membrane disease (TBMD), which primarily involved the glomerulus, not tubular tissue. The diagnosis of TBMD was made according to the general criteria of the average glomerular basement membrane thickness of less than 250 nm.[49] Patient information was anonymized and de-identified before analyses. The entire protocol of the present study was designed in accordance with the Declaration of Helsinki. Due to its retrospective design and low risk to patients, the Ethical Committee approved the use of the following opt-out methodology for the present study. The requirement for verbal informed consent was waived and informed consent was obtained by generally accessible information as well as easy modes to opt-out. This study was approved by the Medical Ethics Committee of the University Hospital of the Kyoto Prefectural University of Medicine (Approval number: ERB-C-2169).

METHOD DETAILS

Patient recruitment and study protocol

We conducted a retrospective cohort study at the University Hospital of the Kyoto Prefectural University of Medicine in Kyoto Prefecture, Japan. We retrospectively enrolled 24 diabetic patients and 4 non-diabetic patients who underwent renal biopsy at Kyoto Prefectural University of Medicine. Clinical characteristics were collected from medical records, including age, sex, complications, primary reason of renal biopsy, laboratory results, which were performed within 2 weeks of the renal biopsy, and are listed in Table S1. The body mass index was defined as [weight (kg)]/[height (meters)]2. eGFR was calculated according to the following formula[48]: "194 × [age (years)]−0.287 × [serum creatinine (mg/dL)]−1.094 × [0.739 if female]". eGFR decline was calculated as the difference from the eGFR one year before the renal biopsy. As a control, we analyzed non-diabetic patients with thin basement membrane disease (TBMD), which primarily involved the glomerulus, not tubular tissue. The diagnosis of TBMD was made according to the general criteria of the average glomerular basement membrane thickness of less than 250 nm.[49] Patient information was anonymized and de-identified before analyses. The entire protocol of the present study was designed in accordance with the Declaration of Helsinki. Due to its retrospective design and low risk to patients, the Ethical Committee approved the use of the following opt-out methodology for the present study. The requirement for verbal informed consent was waived and informed consent was obtained by generally accessible information as well as easy modes to opt-out. This study was approved by the Medical Ethics Committee of the University Hospital of the Kyoto Prefectural University of Medicine (Approval number: ERB-C-2169).

Outcomes

We analyzed composite renal outcomes, including a 40% reduction in eGFR sustained for at least two consecutive measurements, the induction of renal-replacement therapy (maintenance dialysis or renal transplantation), and death from renal causes (defined as death with a proximate renal cause, typically hyperkalemia), which were used in a recent large-scale clinical trial[3] or in our recent retrospective cohort study.[50] The date of 40% reduction in eGFR was defined as the latter date of two consecutive measurements, as mentioned above. The date of the induction of renal replacement therapy was the day of the first dialysis session and day of renal transplantation. The dates of major renal outcomes were ascertained from patient records. All major renal outcomes were confirmed by at least two board-certified nephrologists of the Japanese Society of Nephrology.

Animal experiments

We purchased male diabetic BKS.Cg-Dock7m+/+Leprdb/J (*db/db*) mice and non-diabetic heterozygote (*db/m*) mice aged 6 weeks from Oriental Bio Service Inc. (Kyoto, Japan). 5 mice were housed in one cage under a 12-h light/dark cycle with free access to tap water and standard chow (CE-2, CLEA Japan, Inc., Tokyo, Japan). At the age of 6 weeks, male mice were anesthetized with pentobarbital and unilateral kidney removal was performed by the retroperitoneal approach. One week later, at the age of 7 weeks, mice were anesthetized and resection of upper and lower poles of the right kidney was conducted by the retroperitoneal approach.

For treatment experiments, mice were randomly divided into three groups with the same average blood glucose level at 4 weeks after surgery. Luseogliflozin (3 mg/kg/day, provided by Taisho Pharmaceutical Holdings Co., Ltd., Tokyo, Japan) or 0.5% methyl cellulose as a vehicle was administered to mice by daily oral gavage at 17:00 starting 4 weeks after surgery for 8 weeks. Insulin glargine (0.5 U/kg/day, FUJIFILUM Wako Pure Chemical Corporation, Osaka, Japan) was subcutaneously injected into mice once a day at 17:00. At the indicated time points after surgery, mice were anesthetized with isoflurane and euthanized. After weighing the kidneys, they were cut into samples for further analyses.

Each experimental group contained 5 mice. All experiments were approved by the Experimental Animals Committee, Kyoto Prefectural University of Medicine, and were performed in accordance with the institutional guidelines and Guidelines for Proper Conduct of Animal Experiments by the Science Council of Japan.

Metabolic data

The collection of blood samples and measurements of body weights and BP were performed at 17:00 every 2 weeks. Blood glucose levels and BP were measured by a glucometer (Glutest Every, Sanwa Kagaku Kenkyusho Co., Ltd., Aichi, Japan) and the non-invasive tail cuff method (BP-98A, Softron Co., Ltd., Tokyo, Japan), respectively. Serum BUN levels were assessed using the appropriate enzymatic method (A667-00, Serotec, Hokkaido, Japan).

Regarding 24-h urine collection, mice were placed individually into metabolic cages (KN-645, Natsume Seisakusho Co., Ltd., Tokyo, Japan) every 4 weeks. Urine albumin and creatinine levels were measured using an immunoturbidimetric method (Oriental Yeast Co., Ltd., Tokyo, Japan) and enzyme-linked immunosorbent assay (Nikken Seil Co., Ltd., Shizuoka, Japan), respectively.

Tissue preparation and histological analysis

To obtain paraffin sections, kidneys were fixed with 4% paraformaldehyde and embedded in paraffin by Applied Medical Research Laboratory (Osaka, Japan). Paraffin-embedded mouse and human tissues were cut into 4-μm-thick sections. Periodic Acid-Schiff (PAS) and Masson's trichrome (MTC) staining were performed according to standard procedures. The histology of the kidney was examined using formalin sections stained with PAS and Masson's trichrome. In a histological analysis of human kidney samples, glomerular, interstitial, and vascular lesions were

quantified according to the criteria of the American Society of Nephrology or other international criteria.[26,27] Histology was scored by two nephrologists in a blinded manner, and average scores were calculated for all parameters.

In a histological analysis of murine samples, mesangial expansion was quantified using the following scores: 1, <25%; 2, 25–50%; 3, 50–75%, 4, >75%. The degrees of interstitial fibrosis in MTC-stained kidney sections were scored semi-quantitatively in five random images at 200× magnification. Interstitial fibrosis was quantified using the following scores: 0, 0%; 1, 1–10%; 2, 11–25%; 3, 26–50%; 4, 51–75%; and 5, 76–100%.

Immunohistochemistry

After deparaffinization and antigen retrieval, endogenous peroxidase was quenched with 3.0% hydrogen peroxide in methanol for 20 min. Blocking was performed using 3.0% BSA in PBS for 30 min. Regarding nitrotyrosine staining, blocking was conducted using 1.0% fish gelatin in PBS instead of 3.0% BSA in PBS. Sections were sequentially incubated with primary antibodies, as shown in Table S3, followed by incubation with HRP-conjugated secondary antibodies. Sections were labeled with diaminobenzidine chromogenic substrate (K3468, Agilent Technologies, Inc., Santa Clara, CA), which was used for color visualization, followed by counterstaining with hematoxylin. All sections were observed using an Eclipse E600 microscope (Nikon Corporation, Tokyo, Japan). VCAM1+ tubules in human sections were quantified as a percentage among all tubules. The intensity of podocytes was calculated as a ratio of the number of Wilms tumor 1 (WT1)+ cells to the glomerular area. The number of γH2AX + tubular epithelial cells was quantified by measuring 5–12 HPF images of each kidney section at randomly selected cortical fields. Nitrotyrosine+ tubules were quantified as their percentage among all tubules.

Assessment of renal tissue hypoxia

Tissue hypoxia was visualized and quantified.[10,13,42] In detail, Two hours before sacrifice, luseogliflozin or vehicle was administered to mice by oral gavage. One hour later, pimonidazole (HypoxyprobeTM-1, Natural Pharmacia International, Inc., Burlington, MA) in saline was intraperitoneally injected at a dose of 60 mg/kg. Mice were sacrificed 1 h after the administration of pimonidazole. Pimonidazole was detected by immunohistochemistry (Table S5).

Renal hypoxia was evaluated by the immunostaining of pimonidazole as follows: the percentage of pimonidazole-positive renal tubules in the cortex was calculated by dividing the number of pimonidazole-positive renal tubules by the total number of renal tubules in each field. Hypoxia in the renal cortex was graded by scoring the percentage of pimonidazole-positive renal tubules as follows: 0, 0–9%; 1, 10–29%; 2, 30–49%; and 3, 50–100% as previously described.

Cell culture

Normal rat kidney epithelial cells (NRK 52E cells) were purchased from the JCRB Cell Bank. NRK-52E cells were cultured in Dulbecco's Minimal Essential Medium (Wako, Osaka, Japan) containing 5% fetal bovine serum (Invitrogen Corporation, Carlsbad, CA) at 37°C in a humidified 5% CO2 and 95% air atmosphere. To induce hypoxia, cells were cultured in the gas barrier pouch bag for 6 h using nBIONIX Hypoxic Cell Culture Kit (AR Brown Co., Ltd, Tokyo, Japan). Regarding CoCl2 treatments, 100 μM of CoCl2 was added to the culture medium and incubated for 6 h.

Protein extraction and a Western blot analysis

NRK-52E cell extracts were obtained using lysing Buffer 17 (895943: R&D Systems, Inc. Minneapolis, MN, USA) for 5 min. Proteins were denatured by heating at 95°C for 5 min and separated by SDS-PAGE. Proteins were then transferred onto polyvinylidene difluoride (PVDF) membranes (Immobilon-P IPVH00010: Millipore, MA, USA). After blocking in 5% non-fat milk in TBS/0.1% Tween 20 at room temperature for 1 h, the membrane was incubated with the corresponding primary antibody (Table STAR methods) at 4°C overnight. After washing with TBS/0.1% Tween 20, secondary peroxidase-conjugated anti-rabbit antibodies were added (7076S, 7074S; Cell Signaling Technology, Boston, MA; 1:3000 at room temperature). Chemiluminescence was detected using an ECL select Western blot detection reagent (RPN2235: GE Healthcare UK Ltd., Amersham Place, England) or Clarity Max Western ECL substrate (1705062: Bio-Rad Laboratories, Inc. Hercules, CA, USA). Signal intensities were evaluated using ImageJ software (National Institutes of Health, Bethesda, MD).

RNA extraction and qRT-PCR

Total RNA was extracted from the kidneys or cultured cells using TRIzol (Life Technologies, Inc., Carlsbad, CA) and Direct-zolTM RNA MiniPrep (Zymo Research Corporation., Irvine, CA). Two hundred nanograms of total RNA was reverse transcribed to synthesize cDNA using a PrimeScript RT reagent Kit with a gDNA Eraser (Takara Bio Inc., Shiga, Japan). The real-time detection of PCR products was performed using KAPA SYBR FAST qPCR Master Mix (2×) Universal (Kapa Biosystems, Wilmington, MA) and a Thermal Cycler Dice Real Time System (Takara Bio Inc., Shiga, Japan). All reactions were performed in duplicate. The primers for targets are listed in Table S5.

QUANTIFICATION AND STATISTICAL ANALYSIS

In the mouse study, each experiment was performed using at least five mice per group. Mouse kidney sections were scored semi-quantitatively in five random images by two nephrologists in a blinded manner, and average scores were calculated for all parameters. Statistical analyses were performed using the unpaired t-test to compare two parameters, and the Kruskal-Wallis test to compare multiple parameters. Results are expressed as the mean ± standard error (SE).

In the human study, the Shapiro-Wilk test was used to assess the normal distribution of parameters. A significance level of $p > 0.05$ was considered to be a normal distribution. Statistical analyses were conducted using the unpaired t-test for normally distributed parameters, the Mann-Whitney test for non-normally distributed parameters, and the $\chi 2$-test for dichotomous variables. The mean $\pm$ standard deviation (SD) was used for normally distributed parameters and medians (interquartile range) for non-normally distributed parameters. Survival curves following renal biopsy were analyzed using the Kaplan-Meier method, and a comparison of the high and low VCAM1 groups was performed using the Log rank test. ROC curves were constructed using predictive probability as a covariate and used to compare the sensitivity and specificity of tubular VCAM1 positivity in relation to the incidence of renal outcomes. A significance level of $p < 0.05$ was considered to be significant. Data analyses were performed using GraphPad Prism 8.0 (GraphPad Software Inc., La Jolla, CA, USA).